Triple Helix Formation by α-Oligodeoxynucleotides: A Vibrational Spectroscopy and Molecular Modeling Study

Jean Liquier,‡ Richard Letellier,‡ Cécile Dagneaux,‡ Mohammed Ouali,‡ François Morvan,§ Bernard Raynier,§ Jean Louis Imbach,§ and Eliane Taillandier*,‡

Laboratoire CSSB-URA CNRS 1430, UFR Santé Médecine Biologie Humaine, Université Paris XIII, 74 Rue Marcel Cachin, 93012 Bobigny, France, and Laboratoire de Chimie Bio-Organique, URA CNRS 488, Université Montpellier II, Place E. Bataillon, 34095 Montepellier Cedex, France

Received May 5, 1993; Revised Manuscript Received July 21, 1993®

ABSTRACT: The structures of triple helices $\alpha dT_6{\cdot}\beta dA_n{\cdot}\beta dT_n$, $\alpha dT_{12}{\cdot}\beta dA_n{\cdot}\beta dT_n$, $\alpha dC_{12}^{+}{\cdot}\beta dG_n{\cdot}\beta dC_n$, and $\alpha dC_{12}^{+}{\cdot}\beta rG_n{\cdot}\beta rC_n$ have been studied by Fourier transform infrared spectroscopy, Raman spectroscopy, and molecular mechanics calculations. The sugar conformations in these triplexes have been determined by vibrational spectroscopy. Our results show the existence of only S-type sugars in the $\alpha dT_{12}{\cdot}\beta dA_n{\cdot}\beta dT_n$ triple helix. Both S- and N-type sugar infrared and Raman markers have been detected in the spectra of $\alpha dC_{12}^{+}{\cdot}\beta dG_n{\cdot}\beta dC_n$. Molecular mechanics refinements taking into account vibrational spectroscopy data constraints allow us to propose third strand hydrogen-bonding schemes and third strand polarities in triple helix models. For $\alpha dT_{12}{\cdot}\beta dA_{12}{\cdot}\beta dT_{12}$ the third strand forms reverse Hoogsteen hydrogen bonds with the βdA_{12} strand and therefore is parallel to the purine strand. In contrast, for $\alpha dC_{12}^{+}{\cdot}\beta dG_{12}{\cdot}\beta dC_{12}$ calculations show that only a model in which the third strand is Hoogsteen base paired and antiparallel to the purine strand of the Watson–Crick duplex is compatible with spectroscopic data.

Triple helix formation has recently been extensively studied by a wide variety of techniques in view of the numerous potential applications such as specific regulation of gene expression by antigene nucleic acids or the creation of extremely selective artificial nucleases [for a review, see Hélène and Toulmé (1990)]. Triple helices formed by homopolymers, containing pyrimidine–purine–pyrimidine base triplets (T·A·T, U·A·U, or C^{+}·G·C) have been studied extensively (Howard et al., 1971, 1992; Arnott & Bond, 1973; Arnott & Selsing, 1974; Arnott et al., 1976; Haas & Guschlbauer, 1976; Marck & Thiele, 1978; Thomas & Peticolas, 1983; Miles, 1984; Lewis et al., 1984; de los Santos et al., 1989; Ohms & Ackermann, 1990; Liquier et al., 1991; Hampel et al., 1991; Xodo et al., 1991; Akhebat et al., 1992; Ouali et al., 1993a; Yang & Keiderling, 1993).

However, the potential in vivo use of oligomers to form triple helices is limited in particular due to their degradation by nucleases. A possiblity of nevertheless using oligonucleotides in such native systems is to consider triple helices formed with a third strand containing unnatural oligonucleotides such as phosphorothionates (Latimer et al., 1989; Kim et al., 1992; Rao et al., 1992) or chemically modified bases (Griffin et al., 1992; Froehler & Ricca, 1992; Povsic et al., 1992). Another way is to consider oligonucleotides in which the anomeric configuration of the nucleosides has been changed from β to α. Such anomers are known to be resistant to nucleases both in vitro (Morvan et al., 1986; Thuong et al., 1987; Morvan et al., 1987a) and in vivo (Cazenave et al., 1987). It is thus important to determine whether triple-stranded structures can be formed using α oligomers, to characterize the geometries of such triplexes (Sun & Lavery, 1992) and to compare the information obtained with the data corresponding to similar triplexes formed with natural β oligomers. Vibrational spectroscopy has proved to be a technique particularly well adapted to investigating the secondary structures of nucleic acids and in particular for characterizing the geometries of the sugar moieties (Taillandier et al., 1985; Taillandier & Liquier, 1992).

In this work we present results obtained by vibrational spectroscopy concerning triple helices $\alpha dT_6{\cdot}\beta dA_n{\cdot}\beta dT_n$, $\alpha dT_{12}{\cdot}\beta dA_n{\cdot}\beta dT_n$, $\alpha dC_{12}^{+}{\cdot}\beta dG_n{\cdot}\beta dC_n$, and $\alpha dC_{12}^{+}{\cdot}\beta rG_n{\cdot}\beta rC_n$ (the notation $\alpha dT_6{\cdot}\beta dA_n{\cdot}\beta dT_n$ means that αdT_6 is the third strand bound to the purine strand of the $\beta dA_n{\cdot}\beta dT_n$ Watson–Crick duplex, and similarly for the other studied triple helices).

In the IR spectra of $\alpha dT_6{\cdot}\beta dA_n{\cdot}\beta dT_n$ and $\alpha dT_{12}{\cdot}\beta dA_n{\cdot}\beta dT_n$ triple helices, only S-type (C2′-*endo*) sugars are detected as in the case of the $\beta dT_n{\cdot}\beta dA_n{\cdot}\beta dT_n$ triple helix. However, in contrast to the Hoogsteen base pairing of the β third strand proposed in the $\beta dT_n{\cdot}\beta dA_n{\cdot}\beta dT_n$ triple helix, an IR signature of a reverse Hoogsteen base pairing of the α third strand has been obtained in the $\alpha dT_{12}{\cdot}\beta dA_n{\cdot}\beta dT_n$ triple helix. The infrared and Raman spectra of $\alpha dC_{12}^{+}{\cdot}\beta dG_n{\cdot}\beta dC_n$ show the existence of both S- and N-type sugars (respectively, C2′-*endo* and C3′-*endo* families), the βdGn strand nucleosides adopting the S-type/*anti* geometry.

Molecular mechanics calculations where the sugar conformation was initially forced to experimental vibrational spectroscopy data by an additional energy penalty function allow us to propose accurate models for the third strand polarity and the hydrogen-bonding schemes.

The best model obtained for the $\alpha dT_{12}{\cdot}\beta dA_{12}{\cdot}\beta dT_{12}$ triple helix has reverse Hoogsteen binding of the α third strand with a parallel orientation with respect to the purine strand.

Concerning the $\alpha dC_{12}^{+}{\cdot}\beta dG_{12}{\cdot}\beta dC_{12}$ triple helix, a good agreement with the experimental data has only been obtained for a structure with a Hoogsteen third strand base pairing and a third strand orientation antiparallel to the purine strand.

MATERIALS AND METHODS

Sample Preparation. Polynucleotides, $\beta dG_n{\cdot}\beta dC_n$ (lot AA7890P12) and $\beta dA_n{\cdot}\beta dT_n$ (lot BG7860102) were purchased

* Author to whom correspondence should be addressed.
‡ Université Paris XIII.
§ Université Montpellier II.
® Abstract published in *Advance ACS Abstracts*, September 1, 1993.

0006-2960/93/0432-10591$04.00/0

from Pharmacia, and $\beta rG_n \cdot \beta rC_n$ (lot 56F4022) was purchased from Sigma and used without purification. Oligomers αdC_{12}, αdT_6, and αdT_{12} were prepared and purified as previously described (Morvan et al., 1986).

Triple-stranded structures $\alpha dC_{12}^+ \cdot \beta dG_n \cdot \beta dC_n$ and $\alpha dC_{12}^+ \cdot \beta rG_n \cdot \beta rC_n$, $\alpha dT_6 \cdot \beta dA_n \cdot \beta dT_n$, and $\alpha dT_{12} \cdot \beta dA_n \cdot \beta dT_n$ were obtained by mixing stock solutions of double-stranded polynucleotides ($\beta dG_n \cdot \beta dC_n$, $\beta rG_n \cdot \beta rC_n$, or $\beta dA_n \cdot \beta dT_n$) with the required single strand (αdC_{12}, αdT_6, or αdT_{12}) in a ratio of one phosphate of α third strand per two phosphates of the polymer, i.e., one α base per base pair of the initial duplex. The third strand was heated at 70 °C for 10 min prior to addition so as to avoid aggregation. Then for $\alpha dC_{12}^+ \cdot \beta dG_n \cdot \beta dC_n$ and $\alpha dC_{12}^+ \cdot \beta rG_n \cdot \beta rC_n$ formation, the pH of the mixtures was adjusted to 5.7 by addition of small amounts of HCl. The mixtures were then slowly concentrated down to a volume of 5 μL, and the pH was controlled with a MI4152 microcombination probe from Microelectrodes Inc. For deuteration, samples were slowly evaporated to dryness under nitrogen and then redissolved in the same volume of D_2O. The pH values given in the text or figures are those measured in the H_2O concentrated solutions.

Vibrational Spectroscopy. FTIR spectra were recorded using a Perkin Elmer 1760 Fourier transform spectrophotometer coupled to a PE7700 computer. Usually 20 scans were accumulated. Solution spectra were obtained in ZnSe cells, at a concentration around 100 mM base. Data were treated with the Galaxy Spectra Calc program on an IBM PS2 computer. This treatment included multiple point baseline correction and spectral normalization using the phosphate symmetric stretching vibration found around 1090 cm^{-1} as an internal standard.

Raman spectra were recorded using a Dilor Omars 89 multichannel spectrophotometer. The 514-nm line of a Spectra-Physics Ar^+ laser was used for excitation. Power at the source was 400 mW. Integration time was between 10 and 15 s, and 250 scans were usually accumulated. Data treatment was performed on an IBM AT3 computer using the Dilor multichannel program (multiple point baseline correction and spectral normalization).

Calculations. Molecular modeling of the triplexes $\alpha dC_{12}^+ \cdot \beta dG_{12} \cdot \beta dC_{12}$ and $\alpha dT_{12} \cdot \beta dA_{12} \cdot \beta dT_{12}$, formed by the binding of an α oligonucleotide in the major groove of a $\beta\beta$ duplex, was carried out with the JUMNA IV (Junction Minimization of Nucleic Acid) computer program developed by R. Lavery (Lavery, 1988). Solvent water and counterions were not explicitly included in the calculations. The net charge on each phosphate group was set to $-0.5e$ in order to mimic counterion screening effects. The influence of solvent molecules was simulated by using a sigmoidal distance-dependent dielectric function (Lavery et al., 1986). The triple helices were constructed with 12 base triplets ($n = 12$) in length, so as to simulate the experimental samples where the third strand was a dodecamer. In order to avoid end effects, a mononucleotide symmetry with respect to all helicoidal and internal parameters of each strand was used. Starting structures with Hoogsteen and reverse Hoogsteen third strand hydrogen bondings were considered (Figure 1a–d). The third strand orientation has been taken either parallel or antiparallel to the purine strand of the Watson–Crick duplex. The helicoidal parameters (Xdisp, Ydisp, Inc, tip, twist) used to define the helix structure (Dickerson et al., 1989) were derived from the values given by Arnott for the $\beta dT_n \cdot \beta dA_n \cdot \beta dT_n$ triple helix (Arnott et al., 1976) as previously described (Sun et al., 1991a; Ouali et al., 1993b). Moreover, in each case, starting models

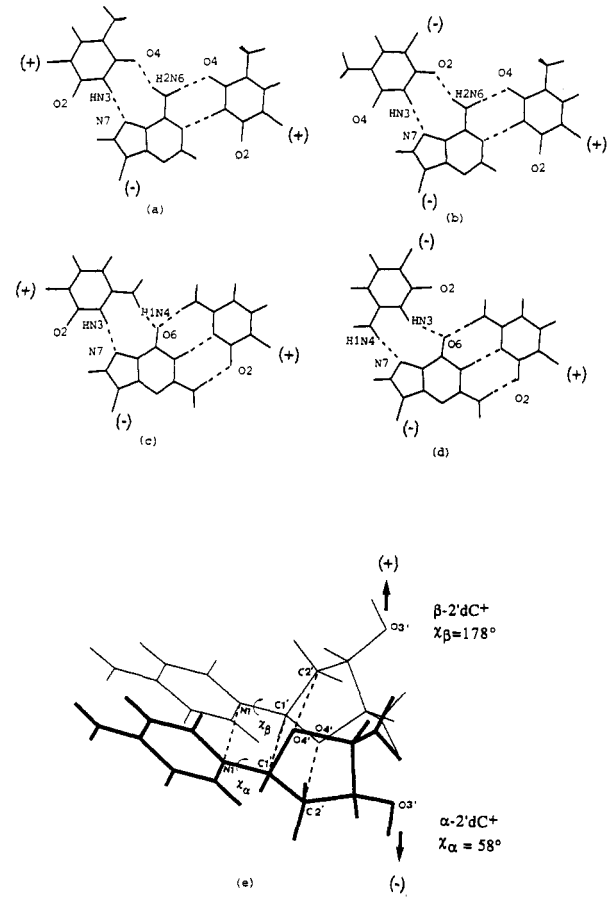

FIGURE 1: Models of $C^+ \cdot G \cdot C$ and T.A.T Triplets. (a) T·A·T triplet with Hoogsteen hydrogen bonding. (b) T·A·T triplet with reverse Hoogsteen hydrogen bonding. (c) $C^+ \cdot G \cdot C$ triplet with Hoogsteen hydrogen bonding. (d) $C^+ \cdot G \cdot C$ triplet with reverse Hoogsteen hydrogen bonding. (e) Comparison between α and β-2′dC+ anomers. The base atoms and the sugar atoms C1′, H1′, O4′, and C2′ of the α anomer are, respectively, superimposed on the base and the C1′, H1′, C2′ and O4′ atoms of the β nucleoside. The symbols (+) and (–) refer to the strand orientation.

were constructed with the sugar–backbone conformation of the three strands derived either from the B-form DNA double helix (Arnott et al., 1980) or from the A-form triple helix (Arnott et al., 1976). The glycosidic torsion angle of the α residue in the third strand was taken either *syn* or *anti*.

During the energy refinement, the sugar pucker conformation was forced to the experimental data by imposing sugar pseudorotation phase angle constraints with the NOE option of JUMNA (Lavery, 1988). After the convergence was achieved, the constraints were relaxed and the structure was minimized again.

In the best calculated model of the $\alpha dC_{12}^+ \cdot \beta dG_{12} \cdot \beta dC_{12}$ triple helix, the deoxyribose sugars of the Watson–Crick duplex were substituted by ribose sugars. The calculated sugar geometry was compared to that deduced from the $\alpha dC_{12}^+ \cdot \beta rG_n \cdot \beta rC_n$ FTIR spectrum.

The molecular structures were visualized with our own interactive computer graphics program "Adngraf" running on a Silicon Graphics workstation.

RESULTS

Vibrational Spectroscopy

$\alpha dT_6 \cdot \beta dA_n \cdot \beta dT_n$ and $\alpha dT_{12} \cdot \beta dA_n \cdot \beta dT_n$ Triplexes. Figure 2 presents the FTIR spectra between 1750 and 1550 cm^{-1} of D_2O solutions of $\beta dA_n \cdot \beta dT_n$ (Figure 2a), αdT_6 (Figure 2b;

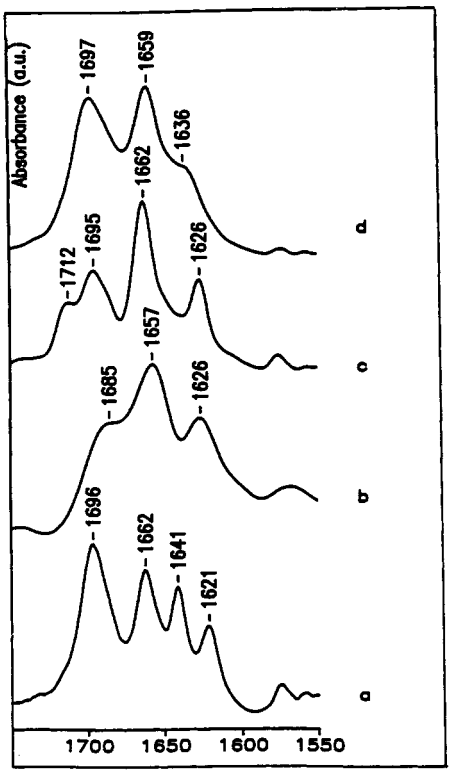

FIGURE 2: D_2O solution FTIR spectra (region of in-plane stretching vibrations of base double bonds): (a) $\beta dA_n \cdot \beta dT_n$. (b) αdT_6. (c) $\alpha dT_{12} \cdot \beta dA_n \beta dT_n$. (d) $\beta dT_n \cdot \beta dA_n \cdot \beta dT_n$.

spectrum shown as reference of nonassociated single-stranded α oligomer), and the $\alpha dT_{12} \cdot \beta dA_n \cdot \beta dT_n$ (Figure 2c) and $\beta dT_n \cdot \beta dA_n \cdot \beta dT_n$ (Figure 2d) triple helices. In this region the in-plane stretching vibrations of the base double bonds are detected. In the $\beta dA_n \cdot \beta dT_n$ spectrum (Figure 2a) the bands at 1696 and 1662 cm^{-1} are assigned to the C2=O2 and C4=O4 carbonyl stretching vibrations of thymines. The absorption observed at 1621 cm^{-1} is assigned to C=C and C=N ring vibrations of adenines coupled to an ND_2 bending vibration (Tsuboi et al., 1962). The formation of the $\beta dT_n \cdot \beta dA_n \cdot \beta dT_n$ triple helix is evidenced by the disappearance of the adenine absorption located at 1621 cm^{-1} and a decrease of the relative intensity of the thymidine band located at 1641 cm^{-1}, as can be seen in Figure 2d (Liquier et al., 1991). The same effect is observed in the case of the $\alpha dT_{12} \cdot \beta dA_n \cdot \beta dT_n$ triplex spectrum (Figure 2c): the adenine absorption at 1621 cm^{-1} is no longer detected, and the relative intensity of the α thymidine band at 1626 cm^{-1} is decreased. Identical results have been obtained by addition to the double-stranded polymer of αdT_6 instead of αdT_{12} (spectra not shown). However, in this spectral region, an additional band can be observed in the FTIR spectra of the triplexes involving α anomers. A contribution is detected at 1712 cm^{-1} (Figure 2c) that is clearly absent in the $\beta dA_n \cdot \beta dT_n$ and in the αdT_6 spectra (Figures 2a,b) as well as in the $\beta dT_n \cdot \beta dA_n \cdot \beta dT_n$ triple helix spectrum (Figure 2d). This suggests a different binding of the third strand in the $\alpha dT_n \cdot \beta dA_n \cdot \beta dT_n$ triplex when compared to the $\beta dT_n \cdot \beta dA_n \cdot \beta dT_n$ triplex. In the Hoogsteen-type base pairing scheme of the T.A.T base triplet (Figure 1a) such as known to occur in the $\beta dT_n \cdot \beta dA_n \cdot \beta dT_n$, both C2=O2 thymine carbonyl groups of the Watson–Crick dT_n strand and of the Hoogsteen dT_n strand are free. On the contrary in a reverse Hoogsteen-type scheme for T.A.T (Figure 1b), the C2=O2 thymine carbonyl groups of the Watson–Crick dT_n strand remain free, but those the reverse Hoogsteen-type dT_n strand are involved in a hydrogen bond. Thus in the spectrum of the

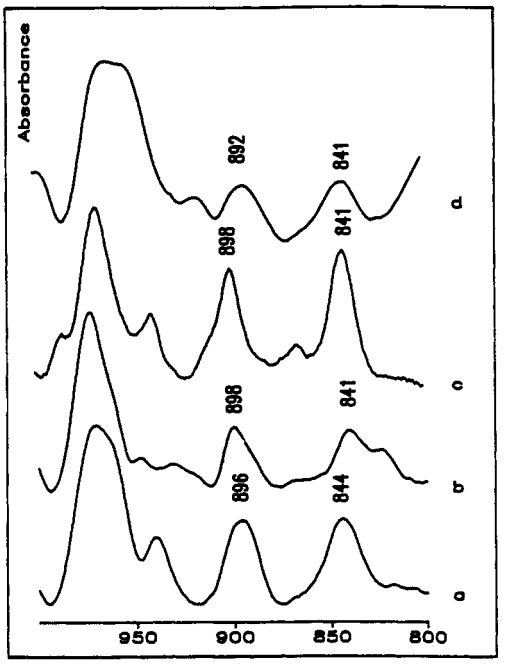

FIGURE 3: D_2O solution FTIR spectra (region of sugar vibrations): (a) poly(dA)·poly(dT), B form. (b) $\beta dT_n \cdot \beta dA_n \cdot \beta dT_n$. (c) $\alpha dT_{12} \cdot \beta dA_n \cdot \beta dT_n$. (d) αd(CGCAATTCGC)·β(GCGTTAAGCG).

$\alpha dT_{12} \cdot \beta dA_n \beta dT_n$ triple helix the two carbonyl absorptions located at 1712 and 1695 cm^{-1} could reflect the existence of two such different C2=O2 carbonyl groups. Moreover, the sum of the relative intensities of these two contributions is similar to that of the unique C2=O2 absorption observed in the case of the $\beta dT_n \cdot \beta dA_n \cdot \beta dT_n$ triple helix. Earlier photo-induced cross-linking and cleavage reaction studies had shown that an oligo-α-thymidilate was bound in the major groove of natural double-stranded DNA in a parallel orientation with respect to the homopurine strand, which was possible only in a model containing reverse Hoogsteen binding of the third strand (Le Doan et al., 1987; Praseuth et al., 1988). The presence of the additional high wavenumber carbonyl vibration in the FTIR spectrum of the $\alpha dT_{12} \cdot \beta dA_n \cdot \beta dT_n$ triple helix allows us to characterize the reverse Hoogsteen-type binding of the αdT_{12} strand to the duplex, in contrast to the Hoogsteen-type binding of the βdT_n strand in the $\beta dT_n \cdot \beta dA_n \cdot \beta dT_n$ triple helix.

The spectral domain between 1000 and 800 cm^{-1} contains absorptions markers of the N-type and S-type sugar geometries. These bands have been widely discussed and used to characterize the A and B families of nucleic acids and the sugar conformations in triplexes (Taillandier & Liquier, 1992; Howard et al., 1992). Figure 3 presents the FTIR spectra of the two $\beta dT_{12} \cdot \beta dA_n \cdot \beta dT_n$ and $\alpha dT_n \cdot \beta dA_n \cdot \beta dT_n$ triple helices (respectively, Figure 3 panels b and c) as well as the spectra of B family form poly(dA)·poly(dT) (Figure 3a) and of an $\alpha\beta$ duplex αd(CGCAATTCGC)·βd(GCGTTAAGCG) (Figure 3d). The latter duplex has been studied by high-resolution 2D NMR (Gmeiner et al., 1992). The NOE data are consistent with a B-form geometry adopted by the α–β hybrid decamer, with S-type sugar pucker and an *anti* conformation for the glycosidic bonds. As can be seen in the FTIR spectrum of this $\alpha\beta$ duplex (Figure 3d), an absorption is observed at 841 cm^{-1} around the same position as the IR marker characteristic of S-type sugars in the case of a $\beta\beta$ duplex (Figure 3a). Thus the S-type sugar conformation IR marker band is the same in the case of $\alpha\beta$ and $\beta\beta$ duplex structures. In the $\alpha dT_{12} \cdot \beta dA_n \cdot \beta dT_n$ triple helix spectrum (Figure 3c) we observe a strong absorption at 841 cm^{-1} which shows that the

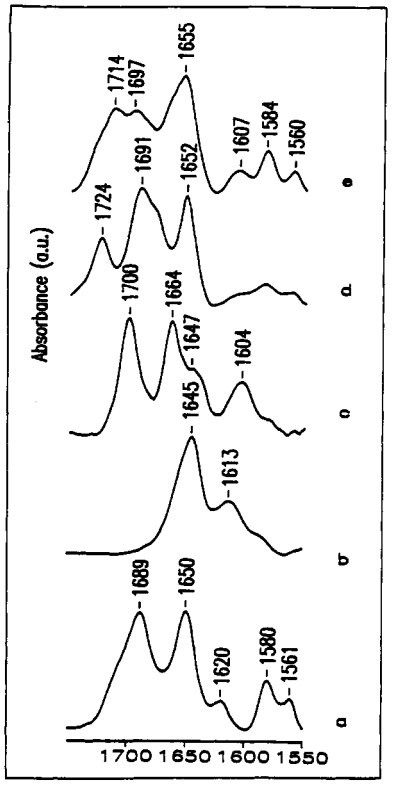

FIGURE 4: D_2O solution FTIR spectra (region of in-plane stretching vibrations of base double bonds): (a) $\beta dG_n \cdot \beta dC_n$. (b) αdC_{12}, pH 7. (c) $\alpha dC_{12}^+ \cdot \alpha dC_{12}$, pH 5.5 (d) $\alpha dC_{12}^+ \cdot \beta dG_n \cdot \beta dC_n$, pH 5.7. (e) $\beta dC_n^+ \cdot \beta dG_n \cdot \beta dC_n$, pH 6.2

sugars are in S-type geometry in all strands. The same sugar conformation had been previously obtained in the case of the $\beta dT_n \cdot \beta dA_n \cdot \beta dT_n$ triplex as can be seen in Figure 3b (Liquier et al., 1991; Howard et al., 1992).

In summary, this study by FTIR spectroscopy allows us to propose for the $\alpha dT_{12} \cdot \beta dA_n \cdot \beta dT_n$ triplex a reverse Hoogsteen type base pairing for the third strand and an S-type sugar conformation for all strands.

$\alpha dC_{12}^+ \cdot \beta dG_n \cdot \beta dC_n$ and $\alpha dC_{12}^+ \cdot \beta rG_n \cdot \beta rC_n$ Triplexes. Figure 4 presents the FTIR spectra of D_2O solutions of $\beta dC_n \cdot \beta dG_n$ at pH 7 (Figure 4a) and of αdC_{12} at pH 8 (Figure 4b) and after decreasing the pH to 5.5 (Figure 4c). So as to obtain the formation of the $\alpha dC_{12}^+ \cdot \beta dG_n \cdot \beta dC_n$ triplex, protonation of the cytosines of the third strand must be achieved by decreasing the pH. The spectrum of the $\alpha dC_{12}^+ \cdot \beta dG_n \cdot \beta dC_n$ triplex obtained at pH 5.7 is shown in Figure 4d. In the $\beta dC_n \cdot \beta dG_n$ spectrum (Figure 4a), two strong absorptions are observed located at 1689 and 1650 cm^{-1}. They are assigned to the coupled stretching vibrations of the C6=O6 guanine and C2=O2 cytosine carbonyl groups. The spectrum of αdC_{12} at pH 8 (Figure 4b) shows one strong band located at 1645 cm^{-1}, assigned to the C2=O2 carbonyl stretching vibration.

The decrease of the pH in β cytidine oligomers or polymers induces formation of different structures depending on the value of the pH. At pH 5.5 (pH value used to form the triple helices studied in this work), double-stranded C^+–C structures have been previously proposed in the case of βdC (Borah & Wood, 1976), βrC_n, or βdC_n (Hartman & Rich, 1965; Chou & Thomas, 1977; Akhebat et al., 1992). At pH 4.5, a four-stranded complex has been recently presented in the case of the d(TCCCCC) oligomer (Gehring et al., 1993). In all cases the protonated cytosines are involved in C^+–C base pair, and all carbonyl groups are hydrogen bonded. The stretching vibration of the C2=O2 group of the protonated hydrogen-bonded cytosines is observed around 1690 cm^{-1} for the βrC^+–βrC and βdC^+–βdC base pairs. When the pH is decreased so as to protonate all the cytosines, the bases are no longer hydrogen bonded, and the spectrum of totally protonated, nonassociated cytosines presents a carbonyl stretching vibration at a still higher wavenumber (around 1713 cm^{-1}). In the same way, the spectrum of the α oligomer at pH 5.5 presented in Figure 4c shows an absorption located at 1700 cm^{-1}, which is indicative of the formation of similar αdC_{12}^+–αdC_{12} structures in the case of α anomers. In the totally protonated αdC_{12}^+ spectrum, the C2=O2 stretching vibration is detected at 1717 cm^{-1} (spectrum not shown).

If we consider the spectrum of the $\alpha dC_{12}^+ \cdot \beta dG_n \cdot \beta dC_n$ triplex (Figure 4d), we can clearly observe a pattern of absorptions due to the stretching vibrations of the carbonyl groups, different from that previously observed for the duplex and for the third strand. This shows the formation of the triple helix between the double-stranded β polymer and the single-stranded α oligomer. The high wavenumber absorption located at 1724 cm^{-1} may be assigned to the stretching vibration of the non-hydrogen-bonded C2=O2 group of the protonated α cytosine of the third strand in the triplex.

The formation of a triple helix by addition of an αdC_{12} oligomer to a $\beta rG_n \cdot \beta rC_n$ duplex and decreasing the pH to 5.7 has been characterized in the FTIR spectrum by a similar emergence of a high wavenumber absorption assigned to the C2=O2 stretching vibration of the protonated α cytosines in the $\alpha dC_{12}^+ \cdot \beta rG_n \cdot \beta rC_n$ triple helix (spectra not shown).

The in-plane base vibration region of the $\alpha dC_{12}^+ \cdot \beta dG_n \cdot \beta dC_n$ and $\alpha dC_{12}^+ \cdot \beta rG_n \cdot \beta rC_n$ triple helix spectra are similar to those previously studied in the case of the triplexes formed with β anomers (Figure 4e). The formation of the triple helix is characterized by the presence of a high wavenumber C2=O2 carbonyl stretching vibration of the protonated cytosine of the third strand.

The absorption of the protonated α cytosine observed at 1724 cm^{-1} in the $\alpha dC_{12}^+ \cdot \beta dG_n \cdot \beta dC_n$ may reflect, as in the case of the $\beta dC_n^+ \cdot \beta dG_n \cdot \beta dC_n$ triplex, a Hoogsteen-type base pairing scheme; however, at this point the reverse Hoogsteen-type model cannot be completely ruled out as in both Hoogsteen and reverse Hoogsteen-type binding schemes of the third strand, the C2=O2 carbonyl of the protonated cytosine remains free (Figure 4c,d). Data provided by the study of the sugar vibrations will allow us to make the base pairing model more precise.

Figure 5 presents FTIR spectra recorded in D_2O solutions between 790 and 920 cm^{-1}, the region where sugar conformation marker modes are observed. The top row shows the spectrum of $\beta dG_n \cdot \beta dC_n$ (Figure 5b) and of the triple helices obtained by addition of a βdC_n^+ (Figure 5d) or of an αdC_{12}^+ (Figure 5f) third strand. The bottom row presents the spectrum of $\beta rG_n \cdot \beta rC_n$ (Figure 5a) and of the triple helices obtained similarly by addition of a βdC_n^+ (Figure 5c) or of an αdC_{12}^+ (Figure 5e) third strand. We can observe in the $\beta rG_n \cdot \beta rC_n$ spectrum (Figure 5a) a band at 862 cm^{-1} characteristic of N-type sugars. In the case of $\beta dG_n \cdot \beta dC_n$ (Figure 5b), the same N-type marker is observed, as in our experimental conditions (high nucleic acid and salt concentrations) this polymer adopts an A family geometry. If we consider the spectrum of $\alpha dC_{12}^+ \cdot \beta dG_n \cdot \beta dC_n$ (Figure 5f), we can detect a contribution of S-type sugars as shown by the existence of an absorption located at 823 cm^{-1}. A similar contribution had been observed in the case of the triple helix formed with a βdC_n third strand (Figure 5d). When a double-stranded RNA is used to form the triple helix, no contribution of S-type sugars

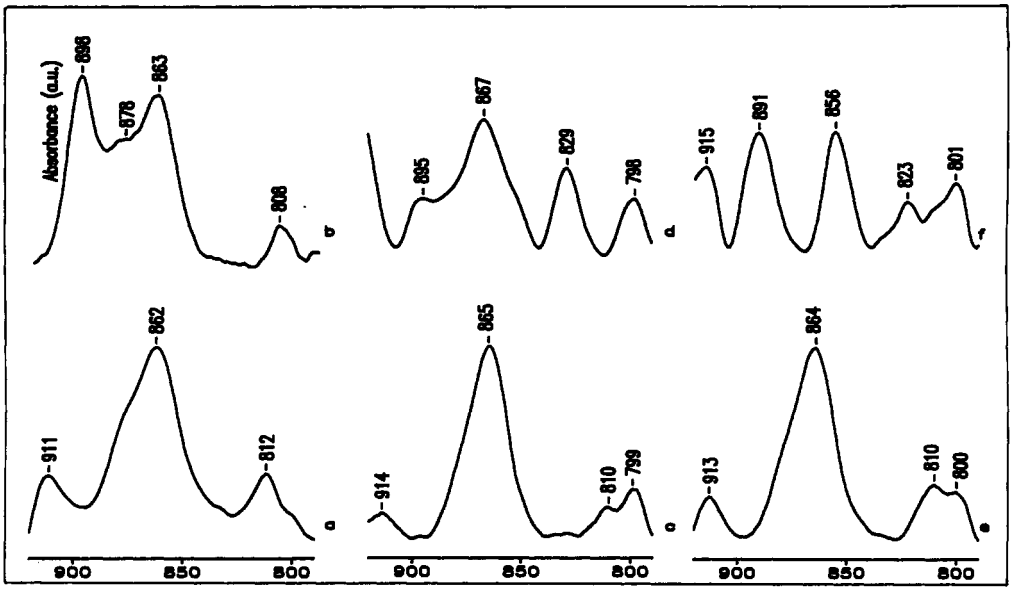

FIGURE 5: D_2O solution FTIR spectra (region of sugar vibrations): (a) $\beta rG_n{\cdot}\beta rC_n$. (b) $\beta dG_n{\cdot}\beta dC_n$. (c) $\beta dC_n^+{\cdot}\beta rG_n{\cdot}\beta rC_n$. (d) $\beta dC_n^+{\cdot}\beta dG_n{\cdot}\beta dC_n$. (e) $\alpha dC_{12}^+{\cdot}\beta rG_n{\cdot}\beta rC_n$. (f) $\alpha dC_{12}^+{\cdot}\beta dG_n{\cdot}\beta dC_n$.

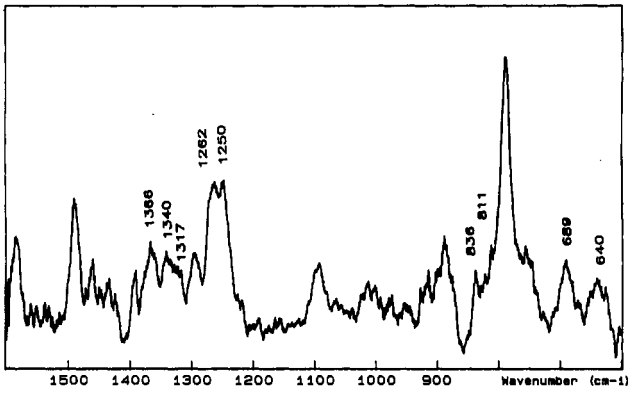

FIGURE 6: Raman spectrum in H_2O solution of $\alpha dC_{12}^+{\cdot}\beta dG_n{\cdot}\beta dC_n$, pH 5.7.

is detected, neither in $\alpha dC_{12}^+{\cdot}\beta rG_n{\cdot}\beta rC_n$ (Figure 5e) nor in $\beta dC_n^+{\cdot}\beta rG_n{\cdot}\beta rC_n$ (Figure 5c).

The Raman spectrum of the $\alpha dC_{12}^+{\cdot}\beta dG_n{\cdot}\beta dC_n$ triple helix is presented in Figure 6. Two regions are of particular interest in this spectrum. The first one between 850 and 600 cm^{-1} contains a vibrational mode of guanosines involving a breathing motion of the imidazole ring coupled through the C1′–N9 glycosidic linkage to a sugar deformation. This mode is known to be a marker of the guanosine conformation: it is observed around 685 cm^{-1} for an S-type/*anti* geometry, around 660 cm^{-1} for an N-type/*anti* conformation and around 625 cm^{-1} for an N-type/*syn* geometry (Thamann et al., 1981; Nishimura et al., 1986; Peticolas et al., 1987). We can observe in the spectrum of the $\alpha dC_{12}^+{\cdot}\beta dG_n{\cdot}\beta dC_n$ triple helix a line located at 689 cm^{-1} and no signal around 660 cm^{-1}, which shows that the guanosines of the βdG_n strand in the triplex adopt an S-type/*anti* geometry.

Moreover, two Raman lines located at 836 and 811 cm^{-1} reflect the existence of S-type and N-type sugars, respectively. The latter can be assigned to the pyrimidine strands as shown by the Raman lines observed between 1400 and 1200 cm^{-1}. The relatively weak triplet located at 1366, 1340, and 1317 cm^{-1} reflects the S-type/*anti* guanosine conformation, whereas the intense line at 1250 cm^{-1} reflects N-type/*anti* cytosines and the companion line at 1262 cm^{-1} the N-type/*anti* protonated cytosines of the third strand (Chou & Thomas 1977; Nishimura et al., 1986). A similar Raman spectrum has been obtained and discussed for the triplex formed with the β anomer in the third strand, $\beta dC_n^+{\cdot}\beta dG_n{\cdot}\beta dC_n$ (Ouali et al., 1993a).

In summary, it is possible to form a triple-helical structure in binding an α oligomer αdC_{12} to double-stranded DNA $\beta dG_n{\cdot}\beta dC_n$. Infrared and Raman spectroscopies show that the β-purine strand adopts an S-type/*anti* geometry whereas pyrimidine strands are in an N-type/*anti* geometry.

Molecular Modeling

Molecular mechanics calculations were performed in order to obtain accurate triplex geometries to enable interpretation of the experimental data. The calculations allow definition of the triplex third strand polarity and hydrogen-bonding schemes which are stereochemically and energetically consistent with the sugar conformations deduced from the vibrational spectra analysis. Calculations clearly show that for $\alpha\beta\beta$ triple helices the Hoogsteen base pairing scheme of the third strand is associated with an antiparallel orientation and the reverse Hoogsteen base pairing scheme with a parallel orientation. In both cases, the third strand glycosidic torsion angle conformation has an *anti* conformation. Other combinations of hydrogen-bonding schemes and third strand polarity (Hoogsteen parallel or reverse Hoogsteen antiparallel and *syn* conformations) have a shorter interstrand backbone distance, and consequently the electrostatic repulsion between the charged phosphates induces an unfavourable stereochemistry.

$\alpha dT_{12}{\cdot}\beta dA_{12}{\cdot}\beta dT_{12}$. When the sugar conformation constraints are relaxed, the best obtained minimized structure of the $\alpha dT_{12}{\cdot}\beta dA_{12}{\cdot}\beta dT_{12}$ triplex involves reverse Hoogsteen third strand base pairing and a parallel third strand polarity. This model is in agreement with the analysis of the 1750–1550-cm^{-1} spectral region (conformation I in Table I; Figure 1b). After the suppression of the energy penalty function, the model with Hoogsteen hydrogen bonds and an antiparallel third strand orientation remains with an S-type sugar conformation, but its energy is significantly higher than the previous one and is thus unfavored (conformation II in Table I).

Table II lists the structural parameters of the reverse Hoogsteen parallel $\alpha dT_{12}{\cdot}\beta dA_{12}{\cdot}\beta dT_{12}$ geometry. The com-

Table I: Comparison between the Sugar Conformations Calculated by Molecular Mechanics for the Triple Helices $\alpha dC_{12}^{+}\cdot\beta dG_{12}\cdot\beta dC_{12}$, $\alpha dC_{12}\cdot\beta rG_{12}\cdot\beta rC_{12}$, and $\alpha dT_{12}\cdot\beta dA_{12}\beta dT_{12}$ and the conformations Obtained by IR and Raman Vibrational Spectroscopies[a]

(N°)	third strand base pairing	third strand orientation	calculated structure	total energy	experimental data
			$\alpha dT_{12}\cdot\beta dA_{12}\cdot\beta dT_{12}$		
I	reverse Hoogsteen	parallel	S/*anti*		S
			S/*anti*	−770	S
			S/*anti* (C3′-*exo*)		S
II	Hoogsteen	antiparallel	S/*anti*		
			S/*anti*	−714	
			S/*anti* (C3′-*exo*)		
			$\alpha dC_{12}^{+}\cdot\beta dG_{12}\cdot\beta dC_{12}$		
III	Hoogsteen	antiparallel	N/*anti*		N
			S/*anti*	−1213	S
			N/*anti* (C2′-*exo*)		N
IV	reverse Hoogsteen	parallel	S/*anti*		
			S/*anti*	−1198	
			S/*anti* (C4′-*endo*)		
			$\alpha dC_{12}^{+}\cdot\beta rG_{12}\cdot\beta rC_{12}$		
V	Hoogsteen	antiparallel	N/*anti*		N
			N/*anti*	−755	N
			N/*anti* (C2′-*exo*)		N

[a] The columns describing the calculated and experimental conformations of triple helices specify, for example in the case of the $\alpha dC_{12}^{+}\cdot\beta dG_{12}\cdot\beta dC_{12}$ triple helix, the sugar pucker and glycosidic torsion angle of the βdC_{12} strand (top), the βdG_{12} strand (middle), and the αdC^{+}_{12} strand (bottom). The S (south), N (north), and W (west) conformations correspond to C2′-*endo*, C3′-*endo*, and O1′-*exo* families, respectively. If the sugar conformation differs from the usual C3′-*endo* or C2′-*endo*, the accurate conformation is given in parentheses.

Table II: Helicoidal Parameters and Conformational Angles of the $\alpha dT_{12}\cdot\beta dT_{12}$ (Conformation I in Table I) and $\beta dT_{10}\cdot\beta dA_{10}\cdot\beta dT_{10}$ (Ouali et al., 1993a) Triple Helix Geometries[a]

	$\alpha dT_{12}\cdot\beta dA_{12}\cdot\beta dT_{12}$					
strand	Xdisp	Ydisp	rise	Inc	tip	twist
I	−1.818	0.073	3.151	−1.547	−8.365	36.81
II	−1.759	−0.001	3.151	5.220	−9.446	36.81
III	−3.562	0.712	3.151	4.457	177.65	36.81

strand	χ	α	β	γ	δ	ε	ζ
I	246	−66	175	60	138	−173	−113
II	253	−62	175	54	140	−172	−115
III	159	−95	131	40	144	−78	−151

	$\beta dT_{10}\cdot\beta dA_{10}\cdot\beta dT_{10}$					
strand	Xdisp	Ydisp	rise	Inc	tip	twist
I	−3.9	0.2	3.4	0.0	0.0	30.9
II	−3.9	0.1	3.4	0.0	0.0	30.9
III	−4.2	−0.3	3.4	0.0	0.0	30.9

strand	χ	α	β	γ	δ	ε	ζ
I	239	−67	−178	55	134	−172	−109
II	238	−62	−179	51	132	−173	−108
III	236	−67	−179	55	129	−172	−105

[a] Strands I, II, and III are, for example in the case of the $\alpha dT_{12}\cdot\beta dA_{12}\cdot\beta dT_{12}$ triplex, βdT_{12}, βdA_{12}, and αdT_{12}, respectively. The helicoidal parameters Xdisp, Ydisp, Inc, and Tip give the position of the base in each strand with respect to a reference point defined as the intersection where the helical axis would cut the base plane in the standard B conformation. The parameters Xdisp and Ydisp are, respectively, the translations along the local dyad axis pointing toward the minor groove and along the long axis oriented following the base pair axis. The Inc and Tip parameters are the rotation parameters around the same two respective axes (Lavery & Sklenar, 1988). Twist, Rise, and conformation torsion angles refer to the usual definitions (IUPAC-IUB, 1983).

Table III: Helicoidal Parameters and Conformational Angles of the $\alpha dC_{12}^{+}\cdot\beta dG_{12}\cdot\beta dC_{12}$ (Conformation III in Table I) and $\alpha dC_{12}^{+}\cdot\beta rG_{12}\cdot\beta rC_{12}$ (Conformation VI in Table I). Optimized Geometries Which Are in Agreement with the Experimental Spectra, and of $\beta dC_{10}^{+}\cdot\beta dG_{10}\cdot\beta dC_{10}$ (Ouali et al., 1993a)[a]

	$\alpha dC_{12}^{+}\cdot\beta dG_{12}\cdot\beta dC_{12}$					
strand	Xdisp	Ydisp	rise	Inc	tip	twist
I	−2.671	−0.269	4.005	−12.75	−4.955	30.26
II	−2.908	0.328	4.005	−9.202	11.973	30.26
III	−4.024	0.268	4.005	−18.636	10.262	30.26

strand	χ	α	β	γ	δ	ε	ζ
I	198	−74	177	69	81	−162	−66
II	239	−61	−173	50	142	−175	−116
III	58	162	−179	−173	99	−176	−72

	$\beta dC_{10}^{+}\cdot\beta dG_{10}\cdot\beta dC_{10}$					
strand	Xdisp	Ydisp	rise	Inc	tip	twist
I	−3.257	−0.256	3.889	−8.725	−4.502	29.64
II	−3.476	0.347	3.889	−8.464	9.555	29.64
III	−4.338	−0.298	3.889	−11.222	4.792	29.64

strand	χ	α	β	γ	δ	ε	ζ
I	198	−72	177	66	80	−161	−66
II	238	−62	−173	51	140	−174	−114
III	186	−76	−179	67	79	−157	−68

	$\alpha dC_{12}^{+}\cdot\beta rG_{12}\cdot\beta rC_{12}$					
strand	Xdisp	Ydisp	rise	Inc	tip	twist
I	−2.860	0.042	4.071	−14.879	−2.763	30.361
II	−3.000	0.084	4.071	−12.855	−1.167	30.361
III	−3.896	−0.024	4.071	−15.278	13.455	30.361

strand	χ	α	β	γ	δ	ε	ζ	C2–O2
I	189	−81	170	79	81	−151	−73	−178
II	190	−85	171	81	83	−152	−72	178
III	60	153	179	−164	101	−177	−71	

[a] The definition of the parameters is the same as in Table II.

parison with the $\beta dT_{10}\cdot\beta dA_{10}\cdot\beta dT_{10}$ triplex (Ouali et al., 1993a) shows that even if the sugar conformation is S-type in both cases and the strand orientations are similar, the helicoidal parameters in the α and β triplexes and the torsion angles ε and ζ are different: the rise is smaller and the twist greater for the triplex containing the α conformer. This corresponds to a difference in the overall helical structure.

$\alpha dC_{12}^{+}\cdot\beta dG_{12}\cdot\beta dC_{12}$. We have performed energy minimization with a penalty energy term imposing an N-type sugar conformation for the two dC strands and an S-type for the dG strand. The results obtained after the contraints have been relaxed show that the $\alpha dC_{12}^{+}\cdot\beta dG_{12}\cdot\beta dC_{12}$ model with a Hoogsteen third strand hydrogen bonding and an antiparallel third strand polarity is the only one in agreement with the experimental infrared and Raman spectra (conformation III in Table I). The other model (with reverse Hoogsteen base pairing and parallel orientation) adopts an S-type sugar conformation when the energy constraint is released (conformation IV in Table I).

For the best $\alpha dC_{12}^{+}\cdot\beta dG_{12}\cdot\beta dC_{12}$ structure, the helicoidal parameters (Xdisp, Ydisp, rise, twist), the sugar conformation, and the backbone torsion angles have values close to those of the $\beta dC_{10}^{+}\cdot\beta dG_{10}\cdot\beta dC_{10}$ triplex (Ouali et al., 1993a) (Table III). The only variations detected concern the Inc parameter and the α torsion angle. Thus the main change observed in the triple helix structure, upon the substitution of the β third strand by an α strand, concerns the third strand polarity, which is antiparallel in the $\alpha dC_{12}^{+}\cdot\beta dG_{12}\cdot\beta dC_{12}$ triplex instead of parallel in the $\beta dC_{10}^{+}\cdot\beta dG_{10}\cdot\beta dC_{10}$ one.

In Table III the values of the χ torsion angle defined as χ O4′–C1′–N1–C2 should be compared between α and β anomers taking into account the following remark: when an

α anomer is considered instead of a β anomer, the H1′ deoxyribose atom is replaced by the N1 pyrimidine atom and this changes the definition of the *syn* and *anti* regions. Considering the same position of the base, an equivalent relative orientation of the sugar with respect to the base for the two α and β anomers is obtained by superimposing the O4′ and C2′ α anomer atoms with, respectively, the C2′ and O4′ atoms of the β anomer (Figure 1e). This leads to the relation $\chi_\alpha = \chi_\beta - 120°$, and the *anti* region is defined in the range $-30° < \chi_\alpha < 150°$ for α anomers instead of $90° < \chi_\beta < 270°$ for β anomers. In Figure 1e is shown the αdC$^+$ anomer of conformation III with an N-type sugar. In this case $\chi_\alpha = 58°$ corresponds to $\chi_\beta = 178°$ in a similar β anomer. We can notice that this value is close to that which had been obtained for βdC$^+$ in the βdC$_{10}^+$·βdG$_{10}^+$·βdC$_{10}^+$ triplex (Table III).

In the best theoretical model (conformation III in Table I), the substitution of the deoxyribose duplex by a ribose duplex gives rise to a refined structure containing only N-type sugars, in good agreement with the IR spectrum of αdC$^+_{12}$·βrG$_n$·βrC$_n$, which presents only one IR marker band at 864 cm^{-1} (conformation V in Table I). The variations of structural parameters induced by the substitution of the deoxyribose duplex by a ribose duplex concern mainly the torsion angle δ of the guanine strand, which is characteristic of the sugar conformation (Table III).

DISCUSSION

In ββ double helices, the modification of the nucleoside anomeric configuration of one strand from β to α without change in the base pairing scheme requires an inversion of the polarity of the α strand (Sun et al., 1987; Lancelot et al., 1987; Morvan et al., 1987b). This is in agreement with our result obtained on αββ and βββ triple helices for which we have shown that if the third base pairing scheme is conserved, an inversion of the third strand orientation is required.

Earlier studies have shown that an oligo-α-deoxythymidilate can bind to a ββ duplex with a parallel orientation (Le Doan et al., 1987). Both α and β oligo(dT) anomers recognize A–T Watson–Crick base pair sequences with the same parallel orientation. In the present work the analysis of the FTIR spectral region between 1750 and 1550 cm^{-1} suggests a reverse Hoogsteen hydrogen-bonding model for the αdT$_{12}$ third strand in the αdT$_{12}$·βdA$_n$·βdT$_n$. Using molecular modeling, we have verified that the experimental conclusions on the parallel third strand polarity and the reverse Hoogsteen base pairing between the αdT$_{12}$ strand and the βDNA were stereochemically compatible with the S-type sugar conformation observed in FTIR spectra of the αdT$_{12}$·βdA$_n$·βdT$_n$ triple helix (conformation I in Table I). This approach based upon the comparison between the calculated sugar conformations of triple helix models and the FTIR data is in agreement with a previous work concerning the αdT$_{10}$·βdA$_{10}$·βdT$_{10}$ triple helix (Sun & Lavery, 1992).

Concerning the αdC$_{12}^+$·βdG$_{12}$·βdC$_{12}$ triple helix, molecular mechanical calculations show that only the calculated model with an Hoogsteen third strand base pairing scheme and an antiparallel third strand polarity can interpret the experimental spectra. These calculations lead us to reject the other possibility, namely, the reverse Hoogsteen parallel αdC$_{12}^+$·βdG$_{12}$·βdC$_{12}$ model which does not give a sugar conformation in agreement with the experimental spectra. Both αdC$_{12}^+$·βdG$_n$·βdC$_n$ and βdC$_{12}^+$·βdG$_n$·βdC$_n$ triple helices have thus a similar Hoogsteen-type base pairing scheme. In the first triplex the α strand is oriented antiparallel to the polypurine strand, whereas in the second triplex the β third strand is oriented parallel to the polypurine strand.

The difference in the orientation of the third strand in the αdC$_{12}^+$·βdG$_n$βdC$_n$ and αdT$_{12}$·βdA$_n$·βdT$_n$ triple helices is consistent with the results of absorption spectroscopy and footprinting assays which have shown that an 11-mer oligonucleotide, 5′-αd(TCTCCTCCTTT)-3′ binds in an antiparallel orientation to a DNA duplex (Sun et al., 1991b). As discussed above, the αdT$_{12}$ oligomer binds with parallel orientation in αdT$_{12}$·βdA$_n$·βdT$_n$, and we can observe that the introduction of αdCs in the αdT third strand induces an inversion of polarity of this strand. This fact could be related to the two different orientations proposed for the αdT$_{12}$ and αdC$_{12}$ strands in our triple helices.

In summary, we have determined the sugar conformations in αdC$_{12}^+$·βdG$_n$·βdC$_n$ and αdT$_{12}$·βdA$_n$·βdT$_n$ triple helices and proposed in the latter case a characterization of a reverse Hoogsteen-type base pairing by the use of vibrational spectroscopy. A conformation has been proposed for each strand involved in the triple helix formation. Molecular mechanics calculations show that only Hoogsteen antiparallel αdC$_{12}^+$·βdG$_{12}$·βdC$_{12}$ and reverse Hoogsteen parallel αdT$_{12}$·βdA$_{12}$·βdT$_{12}$ triple helices can have sugar conformations in agreement with the spectroscopic data. Structural modifications occur by substitution of a β third strand by an α third strand. If the third strand orientation is conserved as in αdT$_{12}$·βdA$_n$·βdT$_n$, then the base pairing scheme is changed; if the base pairing type is invariant as in αdC$_{12}^+$·βdG$_n$·βdC$_n$, then the third strand polarity is reversed.

α Oligonucleotides are resistant to nucleases and can specifically recognize double-stranded DNA sequence motives. This may be of interest in the development of therapeutical approaches such as the inhibition of unwanted gene expression, the so-called genic medication. Our work gives structural information which may be a first step in the design of new drugs based on the anti-gene strategy.

ACKNOWLEDGMENT

We thank Dr. R. Lavery for helpful discussions. Thanks are also due to D. Giroud and J.M. Teuler for their suggestions on the use of the computer facilities at the CIRCE (Centre Inter-Regional de Calcul Electronique, CNRS, Orsay, France).

REFERENCES

Akhebat, A., Dagneaux, C., Liquier, J., & Taillandier, E. (1992) *J. Biomol. Struct. Dyn. 10*, 577–588.

Arnott, S., & Bond, P. J. (1973) *Nature 244*, 99–101.

Arnott, S., & Selsing, E. J. (1974) *J. Mol. Biol. 88*, 509–521.

Arnott, S., Bond, P. J., Selsing, E., & Smith, P. J. C. (1976) *Nucleic Acids Res. 3*, 2459–2470.

Arnott, S., Chandrasekharan, R., Birdsall, R. D. L., Leslie, A. G. W., & Ratliff, R. L. (1980) *Nature 283*, 743–745.

Borah, B., & Wood, J. L. (1976) *J. Mol. Struct. 30*, 13–30.

Cazenave, C., Chevrier, M., Thuong, N. T., & Hélène, C. (1987) *Nucleic Acids Res. 15*, 10507–10520.

Chou, C. H., & Thomas, G. J., Jr. (1977) *Biopolymers 16*, 765–789.

de los Santos, C., Rosen M., & Patel, D. (1989) *Biochemistry 28*, 7282–7289.

Dickerson, R. E., Bansal, M., Calladine, C. R., Dieckman, S., Hunter, N. N., Kennard, O., Lavery, R., Nelson, H. C. M., Olson, W. K., Saenger, W., Shakked, Z. H. S., Soumpasis, D. M., Thung, O. S., Von Kitzing, E., Wang, A. H. J., & Zhurkin, V. B. (1989) *J. Biomol. Struct. Dyn. 6*, 627–634.

Froehler, B. L., & Ricca, D. J. (1992) *J. Am. Chem. Soc. 114*, 8320–8322.

Gehring, K., Leroy, J. L., & Guéron, M. (1993) *Nature 363*, 561–565.

Gmeiner, W. H., Rayner, B., Morvan, F., Imbach, J. L., & Lown, J. W. (1992) *J. Biomol. NMR 2*, 275–288.
Griffin, L. C., Kiessling, L. L., Beal, P. A., Gillespie, P., & Dervan, P. B. (1992) *J. Am. Chem. Soc. 114*, 7976–7982.
Haas, B. L., & Guschlbauer, W. (1976) *Nucleic Acids Res. 3*, 205–218.
Hampel, K. J., Crosson, P., & Lee, J. S. (1991) *Biochemistry 30*, 4455–4459.
Hartman, K. A., & Rich, A. (1965) *J. Am. Chem. Soc. 87*, 2023–2028.
Hélène, C., & Toulmé, J. J. (1990) *Biochim. Biophys. Acta 1049*, 99–125.
Howard, F. B., Frazier, J., & Miles, H. T. (1971) *J. Biol. Chem. 246*, 7073–7086.
Howard, F. B., Miles, H. T., Liu, K., Frazier, J., Raghunathan, G., & Sasisekharan, V. (1992) *Biochemistry 31*, 10671–10677.
IUPAC-IUB Joint Commision On Biochemical Nomenclature (1983) Abbreviations and Symbols for the Description of Conformations of Polynucleotide Chains. *Eur. J. Biochem. 131*, 9–15.
Kim, S. G., Tsukahara, S., Yokoyama, S., & Takaku, H. (1992) *FEBS Lett. 314*, 29–32.
Lancelot, G., Guesnet, J. L., Roig, V., & Thuong, N. T. (1987) *Nucleic Acids Res. 15*, 7531–7547.
Latimer, L. J. P., Hamel, K., & Lee, J. S. (1989) *Nucleic Acids Res. 17*, 1549–1561.
Lavery, R. (1988) *Structure and Expression Vol. 3. DNA Bending and Curvature* (Olson, W. K., Sarma, M. H., Sarma, R. H., & Sundaralingam, M., Eds.) pp 191–211, Adenine Press, Guilderland, NY.
Lavery, R., & Sklenar, H. (1988) *J. Biomol. Struct. Dyn. 6*, 63–91.
Lavery, R., Parker, I., & Kendrick, J. (1986) *J. Biomol. Struct. Dyn. 4*, 443–461.
Le Doan, T., Perrouault, L., Praseuth, D., Habhoub, N., Decout, J. L., Thuong, N. T., Lhomme, J., & Hélène, C. (1987) *Nucleic Acids Res. 15*, 7749–7760.
Lewis, T. P., Miles, H. T., & Becker, E. D. (1984) *J. Phys. Chem. 88*, 3253–3260.
Liquier, J., Coffinier, P., Firon, M., & Taillandier, E. (1991) *J. Biomol. Struct. Dyn. 9*, 437–445.
Marck, C., & Thiele, D. (1978) *Nucleic Acids Res. 5*, 1017–1028.
Miles, M. T. (1984) *Proc. Natl. Acad. Sci. U.S.A. 51*, 1104–1109.
Morvan, F., Rayner, B., Imbach, J. L., Chang, D. K., & Lown, J. W. (1986) *Nucleic Acids Res. 14*, 5019–5035.
Morvan, F., Rayner, B., Imbach, J. L., Lee, M., Hartley, J. A., Chang, D. K., & Lown, J. W. (1987a) *Nucleic Acids Res. 15*, 7027–7044.
Morvan, F., Rayner, B., Imbach, J. L., Thenet, S., Bertrand, J. R., Paoletti, J., Malvy, C., & Paoletti, C. (1987b) *Nucleic Acids Res. 15*, 3421–3437.
Nishimura, Y., Torigoe, C., & Tsuboi, M. (1986) *Nucleic Acids Res. 14*, 2737–2748.
Ohms, J., & Ackermann, T. (1990) *Biochemistry 29*, 5237–5244.
Ouali, M., Letellier, R., Adnet, F., Liquier, J., Sun, J. S., Lavery, R., & Taillandier, E. (1993a) *Biochemistry 32*, 2098–2103.
Ouali, M., Letellier, R., Sun, J. S., Akhebat, A., Adnet, F., Liquier, J., & Taillandier, E. (1993b) *J. Am. Chem. Soc. 115*, 4264–4270.
Peticolas, W. L., Kubasek, W. L., Thomas, G. A., & Tsuboi, M. (1987) in *Biological Applications of Raman Spectroscopy*, (Spiro, T. G., Ed.) Vol. 1, pp 81–133, Wiley, New York.
Povsic, T. J., Strobel, S. A., & Dervan, P. B. (1992) *J. Am. Chem. Soc. 114*, 5934–5941.
Praseuth, D., Perrouault, L., Le Doan, T., Chassignol, M., Thuong, N., & Hélène, C. (1988) *Proc. Natl. Acad. Sci. U.S.A. 85*, 1349–1353.
Rao, T. S., Jayaraman, K., Durland, R. H., & Revankar, G. R. (1992) *Tetrahedron Lett. 33*, 7651–7654.
Roberts, R. W., & Crothers, D. M. (1992) *Science 258*, 1463–1466.
Sun, J. S., & Lavery, R. (1992) *J. Mol. Recognit. 5*, 83–98.
Sun, J. S., Asseline, U., Rouzaud, D., Montenay-Garestier, T., Thuong, N.T., & Hélène, C. (1987) *Nucleic Acids Res. 15*, 6149–6158.
Sun, J. S., Mergny, J. L., Lavery, R., Montenay-Garestier, T., & Hélène, C. (1991a) *J. Biomol. Struct. Dyn. 9*, 411–424.
Sun, J. S., Giovannangeli, C., François, J. C., Kurfurst, K., Montenay-Garestier, T., Asseline, U., Saison-Behmoaras, T., Thuong, N. T., & Hélène, C. (1991b) *Proc. Natl. Acad. Sci. U.S.A. 88*, 6023–6027.
Taillandier, E., & Liquier, J. (1992) *Methods Enzymol. 211*, 307–335.
Taillandier, E., Liquier, J., & Taboury, J. A. (1985) in *Advances in Infrared and Raman Spectroscopy* (Clark, R. H. J., & Hester, R. E., Eds.) Vol. 12, p 65–114, Academic Press, New York.
Thamann, T. J., Lord, R. C., Wang, A. H.-J., & Rich, A. (1981) *Nucleic Acids Res. 9*, 5443–5457.
Thomas, G. A., & Peticolas, W. L. (1983) *J. Am. Chem. Soc. 105*, 993–996.
Thuong, N. T., Asseline, U., Roig, V., Takasigi, M., & Hélène, C. (1987) *Proc. Natl. Acad. Sci. U.S.A. 84*, 5129–5133.
Tsuboi, M., Kyogoku, Y., & Shimanoushi, T. (1962) *Biochim. Biophys. Acta 55*, 1–12.
Xodo, L. E., Manzini, G., Quadrifoglio, F., Van der Marel, G., & Van Boom, J. H. (1991) *Nucleic Acids Res. 19*, 5625–5631.
Yang, L., & Keiderling, T. A. (1993) *Biopolymers 33*, 315–327.